Nanoparticles and Thin Film Formation in Ultrashort Pulsed Laser Deposition of Vanadium Oxide†

Roberto Teghil,*,‡ Luciano D'Alessio,‡ Angela De Bonis,‡ Agostino Galasso,‡ Neluta Ibris,‡ Anna Maria Salvi,‡ Antonio Santagata,§ and Patrizia Villani‡,§

Dipartimento di Chimica, Università della Basilicata, Via N. Sauro 85, 85100 Potenza, Italy, and CNR-IMIP, Unità operativa di Potenza, Via S. Loja, Zona Industriale 85050 Tito Scalo (PZ), Italy

Received: May 30, 2009; Revised Manuscript Received: September 16, 2009

The ultrashort pulsed laser deposition of vanadium oxide thin films has been carried out by a frequency-doubled Nd:glass laser with a pulse duration of 250 fs. The characteristics of the plasma produced by the laser−target interaction have been studied by ICCD imaging and optical emission spectroscopy. The results confirm that an emitting plasma produced by ultrashort laser pulses is formed by both a primary and a secondary component. The secondary component consists of particles with a nanometric size, and their composition and spatial angular distribution influence the deposited films. In fact, these films, analyzed by X-ray photoelectron spectroscopy, X-ray diffraction, scanning electron microscopy, and atomic force microscopy, are formed by the aggregation of a large number of nanoparticles whose composition is explained by a model based on equilibrium thermal evaporation from particles directly ejected from the target. On these basis, the presence in the films of a mixture of V_2O_5 and VO_2 is discussed.

1. Introduction

Pulsed laser deposition (PLD) is a well-known technique, widely used to deposit thin films of materials of a technological interest.[1] PLD can be performed by using both short and ultrashort pulse lasers, and the results are often very different even if the starting material is the same. This is the case, for example, of $Al_{65}Cu_{23}Fe_{12}$ quasi-crystal and TaC. For the first system short pulse PLD leads to films formed by a mixture of quasi-crystalline and metallic alloy phases,[2] while by ultrashort PLD it is possible to obtain films entirely formed by the quasi-crystalline phase.[3] For the second system, on the contrary, the only way to obtain stoichiometric TaC films is to use short pulse PLD.[4] In fact, when the ablation is carried out by an ultrashort pulse laser, the result is the deposition of Ta_2C films.[5] Another recent example of thin film material that is possible to obtain only by ultrashort PLD is rhenium diboride.[6]

Vanadium oxides are a class of materials that are very important for their physicochemical properties.[7] Among these compounds, vanadium pentoxide occupies a special position, especially in the form of a thin film, due to its high potential for the development of electrochromic devices, electronic information displays, and color memory devices.[8,9] V_2O_5 thin films can be deposited by nanosecond PLD only in an oxygen atmosphere. In fact, the deposition performed in vacuum leads to films with a large oxygen deficiency.[10,11] In this paper we have studied the PLD, performed in vacuum by a femtosecond pulse laser, of a V_2O_5 target material with the aim of investigating the ablation-deposition mechanism of a molecular system. The proposed model, already qualitatively applied to tantalum and chromium carbides,[5,12] relates the film morphology and composition to the characteristics of the plasma obtained from the target's ablation.

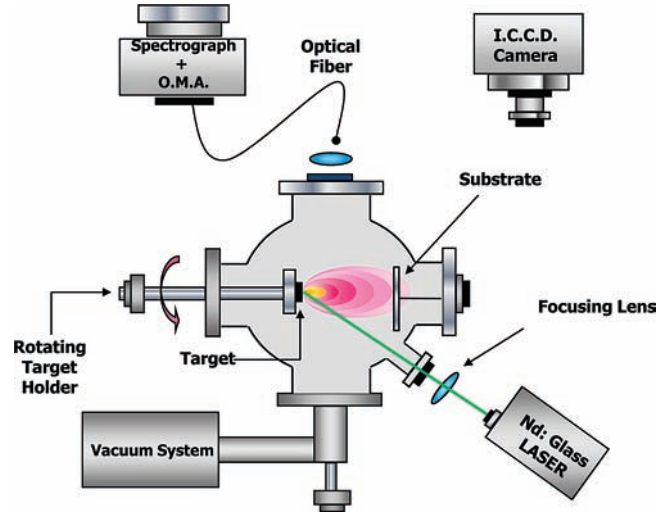

Figure 1. Scheme of the experimental setup.

2. Experimental Section

2.1. Ablation−Deposition Apparatus. The ablation and deposition experiments were performed by using the experimental apparatus shown in Figure 1. It consists of a stainless steel vacuum chamber, evacuated to a pressure of 1.5×10^{-4} Pa, equipped with a rotating target and a heatable substrate holder.

A Light Conversion frequency doubled Nd:glass laser (527 nm emission wavelength, 250 fs pulse duration, 10 Hz repetition rate) was used for the ablation and deposition experiments. The laser fluence was varied between 0.2 and 3.0 J cm^{-2} by changing the laser energy and while maintaining the same spot area (0.1 mm^2).

The laser beam was incident at an angle of 45° on the target surface. The ablation targets were crystalline hot pressed V_2O_5 pellets, and the deposition substrates were (111) oriented silicon

† Part of the "Vincenzo Aquilanti Festschrift".

* Corresponding author: roberto.teghil@unibas.it; tel, +39 0971206249; fax, +39 0971206250.

‡ Dipartimento di Chimica, Università della Basilicata.

§ CNR-IMIP, Unità operativa di Potenza.

10.1021/jp9050947
Published on Web 10/07/2009

from Cerac, FTO coated glass from Solaronix, and ITO-coated glass obtained by a sol−gel method. The substrate temperature was varied between 25 and 500 °C. The target−substrate distance was 6 cm.

2.2. Plasma Characterization. The optical emission spectra were detected using a Princeton ICCD device (1024 × 1024 pixels). The width of the entrance spectrograph slit and the grating employed were of 80 μm and 150 grooves/mm. Thus, the spectral widths obtained were of about 150 nm with resolutions of 0.5 nm. The gated system had best time resolution of 2 ns and each acquisition was integrated over 50 laser shots in order to increase the signal-to-noise ratio. By varying the position of the optical elements by a micrometric translation stage, it has been possible to obtain space-resolved emission spectra at different distances from the ablated target surface. The same ICCD system equipped with 105/35 mm quartz Nikkor lenses was used for acquiring gated, lateral view, images of the overall plasma plume emission (200−800 nm) induced by a single laser pulse. The spatial resolution achieved by this system was 25 μm. The acquisitions were performed by accumulating up to 20 shots, thereby avoiding previously irradiated surfaces. Both ICCD fast imaging and time-resolved spectra were accomplished by delaying the data acquisition of the plasma emission with respect to the laser pulse.

2.3. Thin Films Characterization. The deposits morphological analyses were carried out by a scanning electron microscopy (SEM) apparatus (Philips, FEI ESEM XL30) and by atomic force microscopy (AFM, Park XE 120). X-ray photoelectron spectra (XPS) were acquired by a LH-Leybold 100 spectrometer using unmonochromatized Mg and Al Kα radiations. The curve-fitting procedure was performed with a "Googly" program.[13] The peak assignments were referred to the binding energies to the C 1s signal of aliphatic carbon set at 285.0 eV and based on previous work and published database available online (www.nist.gov).

The films crystallinity was evaluated by X-ray diffraction (XRD, Siemens D5000), using Cu $K\alpha_1$ radiation.

The particle size was measured from AFM images by using Gwyddion 2.16 data analysis software.

2.4. Thermodynamic Calculations. The Fortran program Thermo (B. Ebbinghaus and L. Brewer) was utilized for thermodynamic calculations. This program is designed to calculate the change in Gibbs energy for reactions between the elements and their oxides. The equilibrium constant is also calculated as a function of the temperature. The program also provides an estimate of the uncertainty in both the equilibrium constant and the Gibbs energy.

3. Results and Discussion

3.1. Plasma Analysis. The analysis of the plasma obtained by the laser−target interaction shows the typical features already found in femtosecond ablation.[14] Optical emission spectroscopy (OES) reveals the presence of a primary emission of material, showing the presence of vanadium, neutral and ionized, together with ionized oxygen, with velocities of the order of 10^6 cm s^{-1}. In particular, the velocity of V(I) was 5.0×10^6 cm s^{-1}, while that of O(II) was 7.5×10^6 cm s^{-1}. It was impossible to calculate the velocity of V(II) from the low intensity of the detected signals while the total absence of O(I) emission is probably due to the high intensity of V(I) peaks. An example of the time evolution plots of optical emission in the case of V(I) is reported in Figure 2. After the end of this emission, that lasts less than 1 μs, a second emission of material has been detected, lasting up to 12 μs. This secondary emission shows a blackbody-like spectrum.

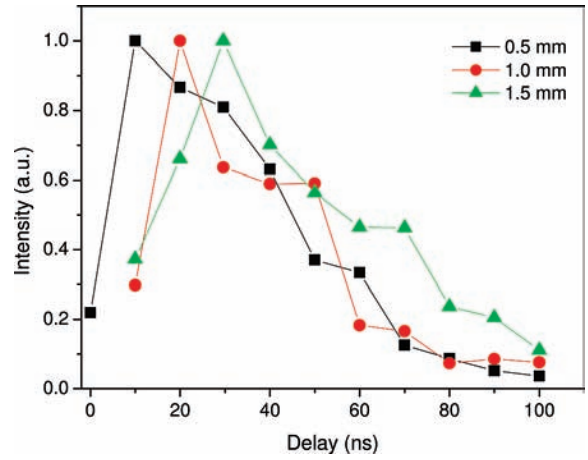

Figure 2. Normalized time evolution plots of the emission of V(I) (471.06 nm), collected 0.5, 1.0, and 1.5 mm from the target. The laser fluence was 3.0 J cm^{-2}. The lines which connect the experimental data were added to facilitate understanding of the graphic.

The measurements of the primary plume velocity, performed by ICCD imaging, give data in good agreement with the OES results. In fact, the velocity of the primary plume front, obtained by considering the position of the plume front in ICCD images recorded at different time delays, is 7.3×10^6 cm s^{-1}, very similar to the velocity of the O(II) particles, the faster particles detected by OES. On the other hand, the velocity of the secondary plume front, calculated in the same way by ICCD imaging, is lower (4.0×10^4 cm s^{-1}) as already found for other systems.[14] In Figure 3 two intensity contour plots, obtained from ICCD images, for the primary (a) and secondary (b) plumes are shown.

The angular distribution of the material ejected from the target during ablation can be represented by the equation $I(\theta) = I_0 \cos^n \theta$, where $I(\theta)$ is the flux intensity along a direction forming an angle θ with the normal to the target surface, I_0 is the intensity corresponding to $\theta = 0$, and n is a parameter related to the anisotropy of the angular distribution. The value of the cosine exponent is $n = 7.2$ for the primary plume and $n = 3.6$ for the second one. The angular distribution of the ejected material is very important since it can influence the shape, thickness, and composition of the deposited films.

The characteristics of the two plumes do not show any significant dependence upon the laser fluence, in the range of our measurements, but there is an increase of the general emission intensity with the raising of the fluence, probably due to the increasing quantity of the ablated material.

3.2. Thin Films Analysis. SEM photomicrographs of the deposited films (Figure 4a) show the presence of a large number of nanoparticles, as already found for all the other systems ablated by ultrashort pulse lasers,[3,5,15−19] but AFM images evidence that the dimension of these nanoparticles can vary from the center to the borders of the deposits. In Figure 4b the morphology of the film center is reported, while Figure 4c shows that of the film border, at a distance of 4.5 cm from the center. It is evident that the particles in the center are smaller, even if aggregated in larger structures. In fact, the particle size distribution, a log-normal distribution in both cases, shows a mean particle diameter of about 45 nm in the center (Figure 5a) and of about 75 nm at the border (Figure 5b).

XRD analyses indicate that the films are always amorphous and XPS spectra of the deposits, reported in Figure 6, give evidence for the presence of vanadium pentoxide and vanadium dioxide peaks. In these spectra the doublets at binding energies

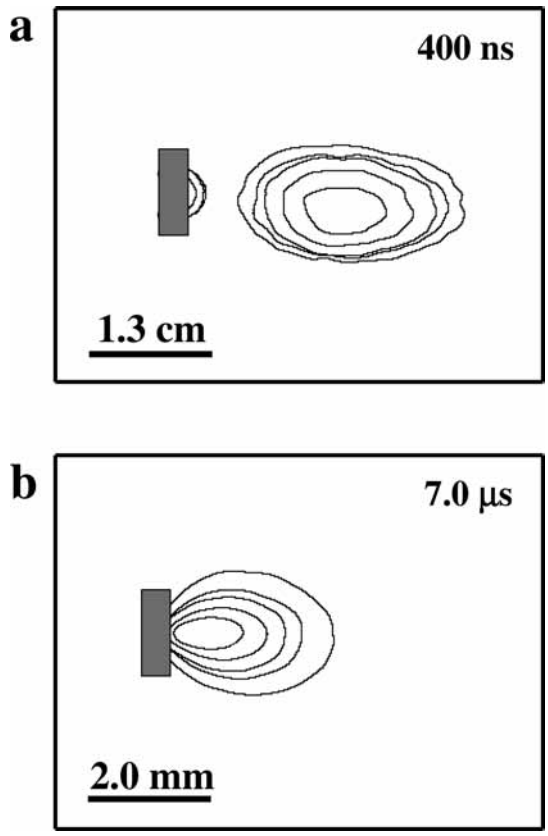

Figure 3. Overall emission from V_2O_5 plumes recorded: (a) 400 ns and (b) 7 μs after the laser shot. The gates were 100 ns in the first case and 500 ns in the second one. The laser fluence was 3.0 J cm^{-2}. The light intensity is shown in terms of 20% density contour plots.

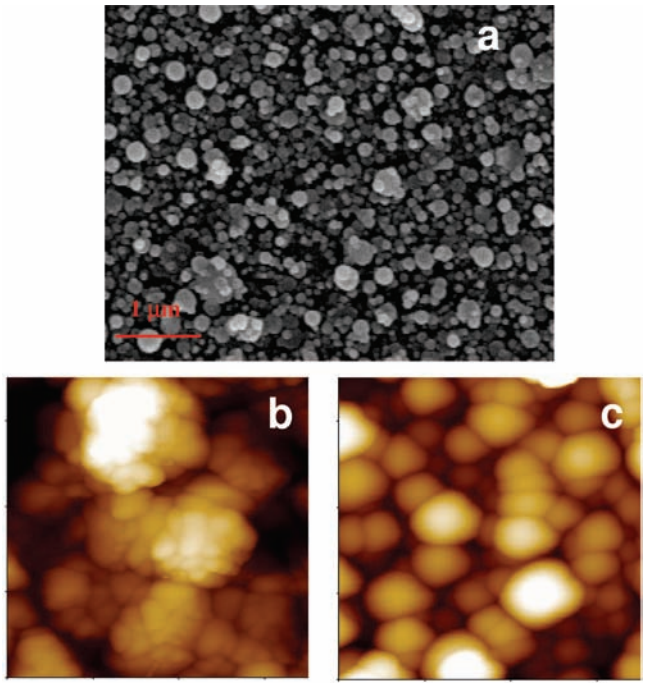

Figure 4. (a) SEM micrograph of the surface of a film obtained by ablation of a V_2O_5 target. The deposition time was 1.5 h and the laser fluence 3.0 J cm^{-2}. AFM image of the surface of the center (b) and of the border (c) of a film obtained by ablation of a V_2O_5 target. The image dimensions are 700 nm × 700 nm. The deposition time was 1.5 h, and the laser fluence 3.0 J cm^{-2}.

(BE) = 517.2 and 524.6 eV ($V^{+5}2p_{3/2}$ and $V^{+5}2p_{1/2}$) and 516.0 and 523.5 eV ($V^{+4}2p_{3/2}$ and $V^{+4}2p_{1/2}$) are assigned to oxygen-

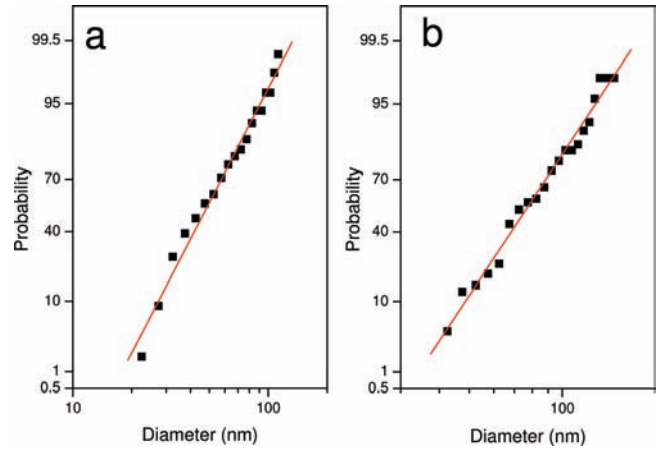

Figure 5. Diameter−probability plots for size distribution of vanadium oxide particles obtained by analysis of AFM images reported in Figure 4: (a) center of the film; (b) border of the film. The solid line fit represents a log-normal size distribution. The value at 50% probability gives the mean value of the particle distribution.

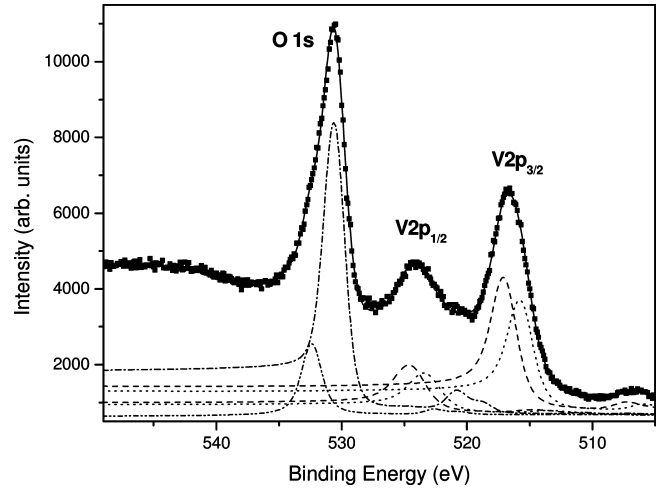

Figure 6. ⟨O 1s V 2p⟩ region of a XPS spectrum of a film obtained by ultrashort PLD of a V_2O_5 target: dashed line, V^{+5} 2p doublet; dotted line, V^{+4} 2p doublet; dotted-dashed line, O 1s bonded to vanadium; double dotted dashed line, O 1s bonded to carbonaceous contaminations. The laser fluence was 3.0 J cm^{-2}.

bonded vanadium, while the peaks at BE 530.7 and 532.4 eV are assigned to vanadium bonded and contamination oxygen, respectively.

None of the film characteristics are changed by changing either the laser fluence or the substrate temperature and are completely independent from the type of substrate.

The data show that the films deposited by femtosecond PLD are composed of both V_2O_5 and VO_2, and this situation is completely different from that found in nanosecond PLD where the films, deposited in vacuum, show a stoichiometry corresponding to VO_{2-x}.[11] The composition of the plume in nanosecond ablation, consisting mainly of vanadium and oxygen, is very similar to that of the femtosecond primary plume and the proposed deposition mechanism is a direct condensation from the gaseous phase.[20]

3.3. Ablation−Deposition Mechanism. The ablation−deposition mechanism producing the morphology found in the femtosecond PLD films is still a matter of debate. In general, there is experimental evidence of the presence of melted material on the target[21,22] and in the expanding plume,[23] so the ablation mechanism should involve the emission of both gaseous material

and melted particles. Some of the possible candidates include, explosive melt removal,[24] phase explosion,[25] and hydrodynamic models.[26] For example, considering the explosive melt removal model, proposed by Tokarev and Kaplan, the parameters of our system satisfy the conditions for a volumetric heating during the target−laser interaction. These conditions are $\chi\tau < 1/\alpha^2$, where χ is the thermal diffusivity, τ the laser pulse duration, and α the absorption coefficient. In our case we have considered[27,28] $\tau = 250$ fs, $\alpha = 2.0 \times 10^4$ cm^{-1}, and $\chi = 5.8 \times 10^{-3}$ cm^2/s. In volumetric laser heating there are two possibilities according to the value of τ_{exp} in comparison with the laser pulse duration τ:

$$\tau_{exp} \ll \tau \quad (1)$$

$$\tau_{exp} \gg \tau \quad (2)$$

In these expressions τ_{exp} is defined as h_0/v_s, where v_s is the velocity of sound in the material and $h_0 = (1/\alpha)\ln(F/F_m)$, F and F_m being the laser energy density incident on the material surface and the melting threshold energy density, respectively. When inequality (1) is satisfied, an equilibrium melting takes place, while in the second case we have a strong nonequilibrium situation. The value of h_0 obtained for our system is 900 nm, leading to $\tau_{exp} = 900$ ps, so, in this case, the inequality (2) is clearly fulfilled. In this situation, the layer h_0 is in a strongly overheated and compressed nonequilibrium state, and one may expect a strong explosive expulsion of the h_0 layer in the form of vapor and molten droplets. In this case the material removal is mainly transverse to the laser spot surface, with the lateral component of material expulsion strongly suppressed,[29] in good agreement with the high directionality of our plumes.

Even considering thin film growth, there is no indubitable evidence about the mechanism, and the relative importance of the material present in primary and secondary plumes is difficult to state. In general, our studies on the variation of the composition with the film angular distribution, in quasi-crystals and metal alloys, indicate a contribution from both primary and secondary plumes, with the larger contribution due to the material from the latter.[30,31] These results are supported by molecular dynamic[19,22] and experimental[32] studies indicating nanoparticles ejected from the target as the main constituents of the plasma and confirmed by the negligible effect of the substrate characteristics on film growth.

Considering the hypothesis that the melted material, produced by one of the nonequilibrium processes mentioned above, could have the target composition, the initial composition of the particles would be the same and every variation would depend on the material loss they might experience during their flight to the substrate. The main material loss mechanism is vaporization from the particle surface, and it depends on the physical properties of the melt and on the temperature. As a consequence of this loss, the particle diameter, a, would change with time as

$$\frac{da}{dt} = -2p\frac{M_v}{\rho RT}\left(\frac{RT}{2\pi M_v}\right)^{1/2} \quad (3)$$

where ρ is the density of the particle, T is the temperature of the particle, p is the vapor pressure, and M_v is the vapor molecular weight.

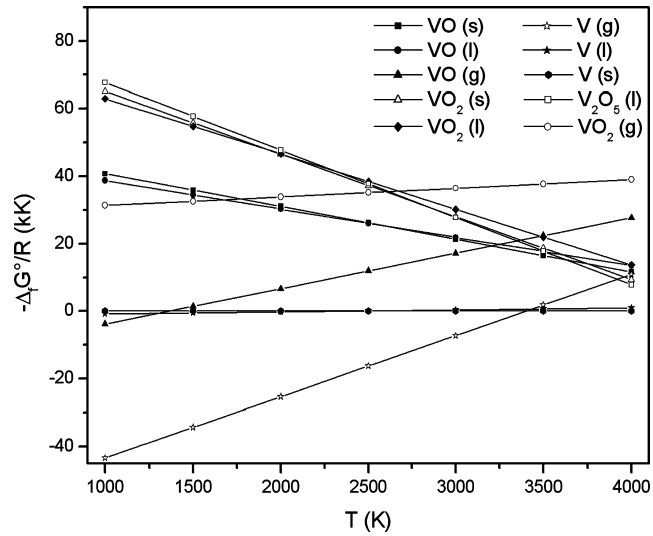

Figure 7. Negative standard Gibbs energy of formation from the elements of the vanadium oxides as a function of the temperature.

In quasi-crystals and metal alloys, the melt retains no memory of the structure of the starting solid material and it can be considered as a solution, either ideal or not. In these cases the material loss, experienced by the molten particle during the flight to the substrate, will actually depend only on the diverse vapor partial pressures of the different elements present in the melt. For $Al_{65}Cu_{23}Fe_{12}$, $Al_{70}Cu_{20}Fe_{10}$, and $Al_{70}Pd_{20}Mn_{10}$ systems the agreement between experiments and calculations has been quite good.[30,31]

When we are in the presence of molecular systems, the situation is different. In this case the material loss from the particles, and so the film composition, will depend on the vaporization thermal equilibriums established in the particles at the different temperatures. Considering the vanadium oxide films deposited by femtosecond PLD, we can explain their composition by studying the thermal vaporization of V_2O_5 at different temperatures.

Thermodynamic calculations have been carried out in order to evaluate the relative stability of the most common vanadium oxides, with respect to the elemental vanadium. The needed data have been obtained by linear extrapolation of lower temperature Gibbs energy values computed by the Fortran program Thermo, utilizing the database included in the program package. The results are shown in Figure 7, where the negative standard Gibbs energies of formation of vanadium oxides are reported as a function of temperature. To facilitate comparison, the data are normalized to a vanadium content of 1 mol in each compound.

To calculate the particles temperature, we have used the OES of the secondary plume that gives the typical blackbody-like spectra, indicating the presence of particles. The temperature data for the secondary plume front have been obtained by fitting the whole UV−vis detected range of secondary plume emissions by the Wien equation ($I_\lambda \propto \varepsilon(1/\lambda^4)e^{-hc/\lambda k_B T}$) at different time delays. Following Mie theory,[33] the emissivity ε of a particle has been calculated by the relation

$$\varepsilon = \frac{4\pi N_m a}{\lambda}\,\mathrm{Im}\left\{\frac{m^2-1}{m^2+2}\right\} \quad (4)$$

where λ is the wavelength of the emitted light, N_m is the refractive index of the medium, $m = N_p/N_m$ where N_p is the refractive index of the particle and a the particle diameter. The

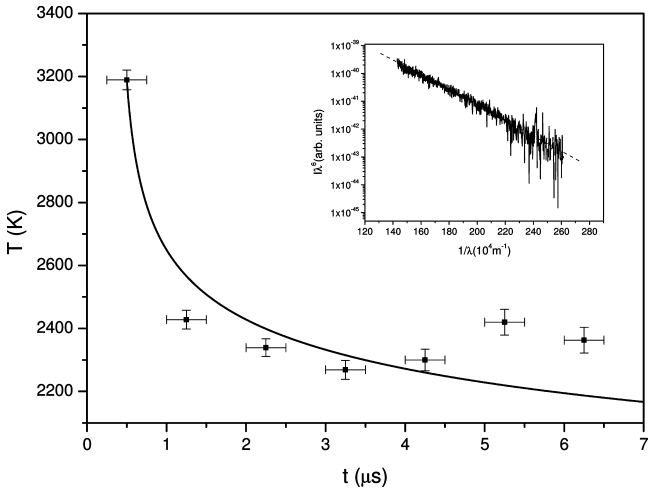

Figure 8. Temporal evolution of the temperature of the secondary plume expanding front. As an example, the inset shows the fitting of a secondary plume emission spectrum giving a temperature of 2270 K. The laser fluence was 3.0 J cm^{-2}. The data are fitted by a cooling curve calculated for a V_2O_5 particle with a diameter of 80 nm.

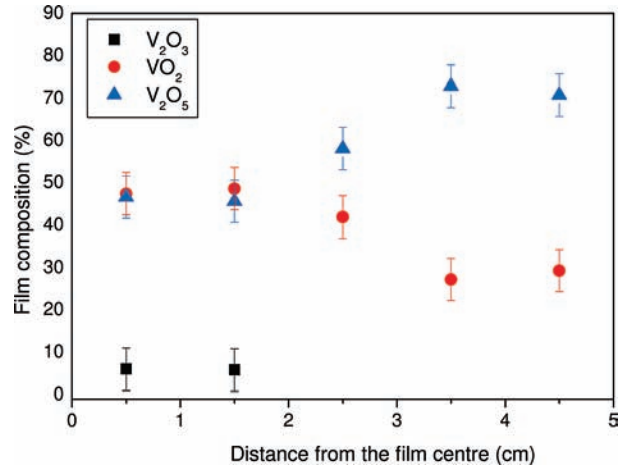

Figure 9. Variation of the film composition as a function of the distance from the film center, obtained by XPS spectra. The points represent the average values recorded on a 1.0 cm^2 area. The deposition time was 1.5 h and the laser fluence 3.0 J cm^{-2}.

results on the plume temperature are reported in Figure 8. The first point corresponds to a distance of 0 mm from the target, a delay of 250 ns after the laser pulse, with a 500 ns gate. The other points have been taken at 0, 0.4, 0.8, 1.2, 1.6, 2.0 mm, with temporal delays of 1, 2, 3, 4, 5, and 6 μs, respectively, while the gate of 500 ns was used in all cases.

The initial temperature is about 3200 K and it decreases to about 2300 K after 6 μs, and this temperature decrease is clearly related to the energy loss experienced by the particles during flight. As already seen for other systems[30,31,34] the main cooling contribution, in this range of temperature and in this time scale, is due to vaporization, and so we have compared the temperature variation of the front of the secondary plume during its expansion with calculations on the particles cooling rate. With this regard, the following cooling rate equation for melted particles has been used, neglecting the radiative and thermionic contributions

$$\frac{dT}{dt} = -\frac{6}{\rho C_p a}\left[p\frac{M_v}{RT}\left(\frac{RT}{2\pi M_v}\right)^{1/2}\frac{\Delta H_v}{M}\right] \quad (5)$$

Here again ρ is the density of the particle, C_p is its thermal capacity, a is the particle diameter, p is the vapor pressure, M_v is the vapor molecular weight, ΔH_v is the vaporization enthalpy, and M is the molecular weight of the particle. In order to determine the temporal dependence of the particle's temperature, this equation, coupled with eq 3 which gives the variation of the particle diameter, has been integrated by the Euler method. The resulting curve, calculated for a particle with an initial diameter of 80 nm is overimposed to the experimental points reported in Figure 8 and confirms that evaporation is the most important cooling process.

The integration of eq 3 alone confirms that vaporization is an important mechanism of material removal for temperatures over 2500 K. From the graph of Figure 7 it is evident that V_2O_5(l) is the most stable species up to about 2500 K, and in any case its stability is comparable to that of VO_2(s,l) over a wide range of temperatures. This indicates that liquid vanadium pentoxide may coexist in equilibrium with the condensed phase of vanadium dioxide up to 3500 K. So whatever the particle initial composition may be, either V_2O_5 or a mixture of V_2O_5 and VO_2, during the flight, there will be an increase of vanadium dioxide percentage at the expense of vanadium pentoxide. In fact the equilibrium between the two species is $V_2O_5(l) \leftrightarrow 2VO_2(l) + {}^1/_2O_2(g)$, even if the material loss is not only due to oxygen production. The presence, in the vapor in equilibrium with liquid V_2O_5 in the temperature range from 1750 to 2250 K, of a large number of different complex species, namely, V_4O_8, V_6O_{14}, V_6O_{12}, V_2O_4 but especially V_4O_{10}, the most abundant,[35,36] indicates that a vanadium loss also takes place.

The presence of particles with different dimensions in the different parts of the films is not surprising. In fact, as reported by Glover,[26] the initial lattice temperature influences the dimensions of the emitted particles, in the sense that a higher temperature corresponds to smaller fragments. The initial target temperature depends on laser fluence and in our case the energy distribution of the laser beam presents a Gaussian profile, giving probably a higher temperature in the center of the spot. A combination of higher temperature and higher surface volume ratio could also affect the evaporation rate from the smaller particles, influencing their composition.

In fact, the relative ratios, V_2O_5/VO_2, on the film surface, obtained by XPS analysis, are not constant but they vary with increase of distance from the film center (Figure 9). This difference in the film composition is attributed to the effect of two different factors, the higher vaporization rate of the small particles in the center of the secondary plume and the different angular distribution of the primary and secondary plumes, both leading to the same result. In fact, the higher vaporization rate of the small particles could move the $V_2O_5-VO_2$ equilibrium in the direction of vanadium dioxide formation. By contrast, the high value of the cosine exponent of the primary plume ($n = 7.2$) indicates that the impact of its highly energetic ions and atoms concerns only the central part of the film. With regard to this, it is well-known that the effect of sputtering by high energetic particles is reduction of the species present on the film surface,[37] so it is not surprising to find the presence of a large amount of VO_2 and even V_2O_3 in the central part of our film. These data confirm again that the deposits are mainly formed by the coalescence of the nanoparticles of the secondary plume, having a large angular distribution ($n = 3.6$).

The low efficiency of the oxidation process for the V_2O_5 system also supports the hypothesis that the films are formed by oxide particles ejected directly from the target. In fact, as

already seen, while in the case of short pulse PLD it was possible to obtain stoichiometric V_2O_5 film by operating in an oxygen atmosphere,[11] this procedure is not so successful in ultrashort PLD since preliminary results show only a slight increase of V_2O_5 percentage, even for quite high oxygen pressure (1500 Pa). The explanation could be found in the difficulty of oxidizing efficiently melted or even solid droplets, while in the case of short pulse PLD the process probably takes place in the gaseous phase.

4. Conclusions

In conclusion, the results obtained on ultrashort PLD of V_2O_5 confirm the previous data on metallic and quasi-crystalline systems. These results indicate that, in the hypothesis that the most important components of the deposited films are nanoparticles, ejected directly from the target, the film composition is related to the material loss from these nanoparticles. The main mechanism of material loss is the thermal vaporization, that the particles experience during their flight to the substrate. In the case of V_2O_5 as starting material, the thermal equilibriums indicate that the particles should be formed of a mixture of vanadium pentoxide and dioxide, and this is exactly the situation we find in the deposited films. Moreover, some film characteristics, such as the variation of the composition from the center to the borders and the different particle size, can also be explained in the same way.

From the point of view of applications, these results seem to confirm some limits of ultrashort PLD. In fact if thermal evaporation from the particles is the most important process influencing the film composition, this technique will eventually experience many of the limitations of the techniques relying on thermal processes.

References and Notes

(1) *Pulsed Laser Deposition of Thin Films: Applications-Led Growth of Functional Materials*; Eason, R., Ed.; Wiley-Interscience: Hoboken, NJ, 2007.

(2) Teghil, R.; D'Alessio, L.; Simone, M. A.; Zaccagnino, M.; Ferro, D.; Sordelet, D. J. *Appl. Surf. Sci.* **2000**, *168*, 267.

(3) Teghil, R.; D'Alessio, L.; Santagata, A.; Zaccagnino, M.; Ferro, D.; Sordelet, D. J. *Appl. Surf. Sci.* **2003**, *210*, 307.

(4) Teghil, R.; D'Alessio, L.; Zaccagnino, M.; Ferro, D.; Marotta, V.; De Maria, G. *Appl. Surf. Sci.* **2001**, *173*, 233.

(5) Teghil, R.; De Bonis, A.; Galasso, A.; Villani, P.; Santagata, A. *Appl. Surf. Sci.* **2007**, *254*, 1220.

(6) Latini, A.; Rau, J. V.; Ferro, D.; Teghil, R.; Rossi Albertini, V.; Barinov, S. M. *Chem. Mater.* **2008**, *20*, 4507.

(7) Surnev, S.; Ramsey, M. G.; Netzer, F. P. *Prog. Surf. Sci.* **2003**, *73*, 117.

(8) Granqvist, C. G.; *Handbook of Inorganic Electrochromic Materials*; Elsevier: Amsterdam, 1995.

(9) Alamarguy, D.; Castle, J. E.; Ibris, N.; Salvi, A. M. *J. Vac. Sci. Technol., A* **2007**, *25*, 1577.

(10) Ramana, C. V.; Smith, R. J.; Hussain, O. M.; Julien, C. M. *Mater. Sci. Eng., B* **2004**, *111*, 218.

(11) Bowman, R. M.; Gregg, J. M. *J. Mater. Sci.: Mater. Electron.* **1998**, *9*, 187.

(12) Teghil, R.; Santagata, A.; De Bonis, A.; Galasso, A.; Villani, P. *Appl. Surf. Sci.* **2009**, *255*, 7729.

(13) Castle, J. E.; Salvi, A. M. *J. Electron Spectrosc. Relat. Phenom.* **2001**, *114*−*116*, 1103.

(14) Albert, O.; Roger, S.; Glinec, Y.; Loulergue, J. C.; Etchepare, J.; Boulmer-Leborgne, C.; Perriere, J.; Millon, E. *Appl. Phys. A: Mater. Sci. Process.* **2003**, *76*, 319.

(15) Eliezer, S.; Eliaz, N.; Grossman, E.; Fisher, D.; Gouzman, I.; Pecker, S.; Horovitz, Y.; Fraenkel, M.; Maman, S.; Lereah, Y. *Phys. Rev. B* **2004**, *69*, 144119.

(16) Scuderi, D.; Benzenga, R.; Albert, O.; Reynier, B.; Etchepare, J. *Appl. Surf. Sci.* **2006**, *252*, 4360.

(17) Bulgakov, A. V.; Ozerov, I.; Marine, W. *Appl. Phys. A: Mater. Sci. Process.* **2004**, *79*, 1591.

(18) Teghil, R.; D'Alessio, L.; De Bonis, A.; Galasso, A.; Villani, P.; Santagata, A. *Thin Solid Films* **2006**, *515*, 1411.

(19) Nedialkov, N. N.; Atanasov, P. A.; Amoruso, S.; Bruzzese, R.; Wang, X. *Appl. Surf. Sci.* **2007**, *253*, 7761.

(20) Flamini, C.; Ciccioli, A.; Giardini Guidoni, A.; Mele, A. *J. Mater. Synth. Process.* **2001**, *9* (3), 143.

(21) Okano, Y.; Oguri, K.; Nishikawa, T. *Appl. Phys. Lett.* **2006**, *89*, 22150.

(22) Perez, D.; Lewis, L. J. *Phys. Rev. B* **2003**, *67*, 184102.

(23) Okano, Y.; Oguri, K.; Nishikawa, T.; Nakano, H. *J. Phys: Conf. Ser.* **2007**, *59*, 769.

(24) Tokarev, V. N.; Kaplan, A. F. H. *Laser Eng.* **1998**, *7*, 295.

(25) Miotello, A.; Kelly, R. *Appl. Phys. A: Mater. Sci. Process.* **1999**, *69*, S67.

(26) Glover, T. E. *J. Opt. Soc. Am. B* **2003**, *20*, 125.

(27) Wu, G.; Du, K.; Xia, C.; Kun, X.; Shen, J.; Zhou, B.; Wang, J. *Thin Solid Films* **2005**, *485*, 284.

(28) Fedorov, V. I.; Davydov, I. I. *High Temp.* **1979**, *16*, 654.

(29) Tokarev, V. N.; Kaplan, A. F. H. *J. Phys. D: Appl. Phys.* **1999**, *32*, 1526.

(30) Teghil, R.; De Bonis, A.; Galasso, A.; Santagata, A.; Villani, P.; Sordelet, D. J. *Chem. Phys. Lett.* **2007**, *438*, 85.

(31) Teghil, R.; D'Alessio, L.; De Bonis, A.; Ferro, D.; Galasso, A.; Lanza, G.; Santagata, A.; Villani, P.; Sordelet, D. J. *Thin Solid Films* **2009**, *517*, 1880.

(32) Hermann, J.; Noel, S.; Itina, T. E.; Axente, E.; Povarnitsyn, M. E. *Laser Phys.* **2008**, *18*, 374.

(33) Bohren, C. F.; Huffman, D. R. *Absorption and Scattering of Light by Small Particles*; Wiley: New York, 1983.

(34) Heszler, P.; Elihn, K.; Landstrom, L.; Boman, M. *Smart Mater. Struct.* **2002**, *11*, 631.

(35) Farber, M.; Uy, O. M.; Srivastava, R. D. *J. Chem. Phys.* **1972**, *56*, 5312.

(36) Herwig, C; Limberg, C. *Inorg. Chem.* **2008**, *47*, 2937.

(37) Mitchell, D. F.; Sproule, G. I.; Graham, M. J. *Surf. Interface Anal.* **2004**, *15*, 487.

JP9050947